INTERNATIONAL JOURNAL FOR NUMERICAL METHODS IN FLUIDS
Int. J. Numer. Meth. Fluids 2007; **55**:1143–1155
Published online 15 May 2007 in Wiley InterScience (www.interscience.wiley.com). DOI: 10.1002/fld.1520

The dispersal processes within the tide-modulated Changjiang River plume, China

Li-Feng Lu and John Z. Shi*, †

School of Naval Architecture, Ocean and Civil Engineering, Shanghai Jiao Tong University, 1954 Hua Shan Road, Shanghai 200030, China

SUMMARY

The dispersal processes of the tide-modulated Changjiang River plume, China, are studied by using a three-dimensional hydrodynamical module of the COHERENS (A COupled Hydrodynamical–Ecological model for REgional and Shelf Seas). The model is driven by the river discharge and the M_2 tidal constituent. Modelled results show: (1) the fresh water, which forms the Changjiang River plume expanding southeastwards, is discharged mostly into the North Channel, the North Passage, and the South Passage; (2) the larger horizontal gradient outside the North Channel and the North Passage forms a strong plume front; (3) the Changjiang River plume is homogeneous vertically, and dispersing gradually within the computational domain, with an averaged propagating rate of 3.38 km/day, while the plume front is surface-to-bottom type, and trapped between −10 and −18 m isobaths; and (4) both the plume length and the plume front intensity vary periodically. The maximum plume length occurs about 2 h after low slack water and the minimum plume length during high slack water. The maximum plume front intensity occurs during high slack water and the minimum plume front intensity during low slack water. Copyright © 2007 John Wiley & Sons, Ltd.

Received 23 January 2007; Revised 27 March 2007; Accepted 4 April 2007

KEY WORDS: dispersion; tide-modulated; salinity; Changjiang River plume

1. INTRODUCTION

'When the Froude number at the river mouth is less than critical, the brackish surface layer will be able to penetrate seawards of the mouth as a plume, especially during the ebb tide' [1]. Many estuarine plumes have been found around the world, e.g. the Amazon River estuary, Brazil [2]; the

*Correspondence to: John Z. Shi, School of Naval Architecture, Ocean and Civil Engineering, Shanghai Jiao Tong University, 1954 Hua Shan Road, Shanghai 200030, China.
†E-mail: zshi@sjtu.edu.cn

Contract/grant sponsor: National Science Fund for Distinguished Young Scholars; contract/grant number: 40225014
Contract/grant sponsor: National Natural Science Foundation of China; contract/grant number: 50679040

Columbia River estuary [3–5] and the Connecticut River estuary [6, 7], U.S.A.; the Pearl River estuary [8], China; the Rhine River estuary [9–11], the Netherlands; and the Rhone River estuary [12], France.

The Changjiang River is the largest river in Asia and fifth largest in the world in terms of annual mean volume discharge (about $3.0 \times 10^4\ m^3\ s^{-1}$) [13]. The huge volume of fresh water empties to the Yellow and East China Sea, and forms a remarkable plume, which influences not only the circulation and suspended sediment transport in the Hangzhou Bay [14], but also the salinity distribution in the Japan Sea [15]. Its estuary is divided by the Chongming Island into the North Branch and the South Branch. The South Branch is further divided into the North Channel and the South Channel, while the latter is divided into the North Passage and the South Passage (Figure 1).

Both observational and numerical modelling efforts have been made to the Changjiang River plume. Beardsley *et al*. [13, 16] observed the structure of the Changjiang River plume. It was found that the Changjiang River plume exhibits a bimodal distribution in the summer, with a part of fresh water extending southwards, and the rest extending offshore on average towards northeast; while in the winter, it spreads southwards in a narrow band along the coast. Zhang *et al*. [17] developed an analytical model to understanding flow conditions and estuarine plume distributions in the Changjiang River estuary. Su and Wang [14] found a secondary plume front at the south boundary of the Changjiang River plume that serves as a guide for sediment transport. Bang and Lie [18] simulated the Changjiang River plume with realistic geography and topography, and indicated that the topography of the Changjiang Estuary suppresses the offshore expansion of the plume water, but does not hinder it from spreading along the coast. The dispersion of the Changjiang River plume is very sensitive to wind conditions. Lie *et al*. [19] indicated that the plume in the mid-shelf is confined to a thin surface layer 10–15 m thick in the summer, extending eastwards in the form of patches of low-salinity water rather than spreading as a tongue-shaped pattern from the Changjiang mouth. Chang and Isobe's [15] simulation showed a remarkable seasonal variation of the Changjiang diluted water, and pointed out that the eastward extension of the Changjiang diluted water is strongly constrained by the Taiwan-Tsushima Warm Current System over the shelf regime. Wang [20] presented an overview of cultural eutrophication within the Changjiang River plume. However, little information is available on the dispersal processes of the tide-modulated Changjiang River plume.

This paper attempts to better understand the dispersal processes of the tide-modulated Changjiang River plume and its associated plume front over a tidal cycle in the summer by using numerical modelling. Apparently, the Prince Ocean Model was generally used for the Changjiang River plume in other numerical modelling studies, e.g. Chang and Isobe [15] and Bang and Lie [18]. This paper will use a three-dimensional hydrodynamical module of the COHERENS (A COupled Hydrodynamical-Ecological model for REgional and Shelf Seas). Preliminary results of an incomplete early version were presented at the ICEC 2006 [21].

2. DETAILS OF MODEL AND ITS CONFIGURATION

A three-dimensional hydrodynamical module of the COHERENS model [22] is used to understand the dispersal processes of the tide-modulated Changjiang River plume. This model uses a mode-splitting technique to solve the two-dimensional barotropic and three-dimensional baroclinic equations on the staggered horizontal meshes of 140×188, with 10 sigma vertical levels.

DOI: 10.1002/fld

Internal model:
Continuity equation:

$$\frac{\partial u}{\partial x}+\frac{\partial v}{\partial y}+\frac{\partial w}{\partial z}=0 \tag{1}$$

Momentum equation:

$$\begin{aligned}&\frac{\partial u}{\partial t}+u\frac{\partial u}{\partial x}+v\frac{\partial u}{\partial y}+w\frac{\partial u}{\partial z}-fv\\&\quad=-\frac{1}{\rho_0}\frac{\partial p}{\partial x}+2\nu_{\mathrm{H}}\frac{\partial^2 u}{\partial x^2}+\nu_{\mathrm{H}}\frac{\partial}{\partial y}\left(\frac{\partial u}{\partial y}+\frac{\partial v}{\partial x}\right)+\frac{\partial}{\partial z}\left(\nu_{\mathrm{T}}\frac{\partial u}{\partial z}\right)\end{aligned} \tag{2}$$

$$\begin{aligned}&\frac{\partial v}{\partial t}+u\frac{\partial v}{\partial x}+v\frac{\partial v}{\partial y}+w\frac{\partial v}{\partial z}+fu\\&\quad=-\frac{1}{\rho_0}\frac{\partial p}{\partial y}+\nu_{\mathrm{H}}\frac{\partial}{\partial x}\left(\frac{\partial u}{\partial y}+\frac{\partial v}{\partial x}\right)+2\nu_{\mathrm{H}}\frac{\partial^2 v}{\partial y^2}+\frac{\partial}{\partial z}\left(\nu_{\mathrm{T}}\frac{\partial v}{\partial z}\right)\end{aligned} \tag{3}$$

$$\frac{\partial p}{\partial z}=-\rho g \tag{4}$$

Salinity equation:

$$\frac{\partial S}{\partial t}+u\frac{\partial S}{\partial x}+v\frac{\partial S}{\partial y}+w\frac{\partial S}{\partial z}=\frac{\partial}{\partial x}\left(\lambda_{\mathrm{H}}\frac{\partial S}{\partial x}\right)+\frac{\partial}{\partial y}\left(\lambda_{\mathrm{H}}\frac{\partial S}{\partial y}\right)+\frac{\partial}{\partial z}\left(\lambda_{\mathrm{T}}\frac{\partial S}{\partial z}\right) \tag{5}$$

where u, v, w are the components of velocity in the x, y, and z directions, respectively; t is the time; f is the Coriolis force; ρ_0 is the reference density; ν_{H} is the horizontal diffusivity; ν_{T} is the vertical eddy viscosity; p is the pressure; ρ is the water density; g is the gravity acceleration; S is the salinity; λ_{H} and λ_{T} are the horizontal and vertical diffusivities, respectively.

External model:
Continuity equation:

$$\frac{\partial \zeta}{\partial t}+\frac{\partial \overline{U}}{\partial x}+\frac{\partial \overline{V}}{\partial y}=0 \tag{6}$$

Momentum equation:

$$\begin{aligned}&\frac{\partial \overline{U}}{\partial t}+\frac{\partial}{\partial x}\left(\frac{\overline{U}^2}{H}\right)+\frac{\partial}{\partial y}\left(\frac{\overline{U}\,\overline{V}}{H}\right)-f\overline{V}+gH\frac{\partial \zeta}{\partial x}\\&\quad=\overline{Q}_1+\frac{1}{\rho_0}(\tau_{\mathrm{s1}}-\tau_{\mathrm{b1}})+2\overline{\nu}_{\mathrm{H}}\frac{\partial^2}{\partial x^2}\left(\frac{\overline{U}}{H}\right)+\overline{\nu}_{\mathrm{H}}\frac{\partial}{\partial y}\left[\frac{\partial}{\partial y}\left(\frac{\overline{U}}{H}\right)+\frac{\partial}{\partial x}\left(\frac{\overline{V}}{H}\right)\right]\end{aligned} \tag{7}$$

$$\begin{aligned}&\frac{\partial \overline{V}}{\partial t}+\frac{\partial}{\partial x}\left(\frac{\overline{U}\,\overline{V}}{H}\right)+\frac{\partial}{\partial y}\left(\frac{\overline{V}^2}{H}\right)+f\overline{U}+gH\frac{\partial \zeta}{\partial y}\\&\quad=\overline{Q}_2+\frac{1}{\rho_0}(\tau_{\mathrm{s2}}-\tau_{\mathrm{b2}})+\overline{\nu}_{\mathrm{H}}\frac{\partial}{\partial x}\left[\frac{\partial}{\partial y}\left(\frac{\overline{U}}{H}\right)+\frac{\partial}{\partial x}\left(\frac{\overline{V}}{H}\right)\right]+2\overline{\nu}_{\mathrm{H}}\frac{\partial^2}{\partial y^2}\left(\frac{\overline{V}}{H}\right)\end{aligned} \tag{8}$$

DOI: 10.1002/fld

where $\overline{U} = \int_{-h}^{\zeta} u\,\mathrm{d}z$ and $\overline{V} = \int_{-h}^{\zeta} v\,\mathrm{d}z$ are the water depth-integrated components of velocity in the x and y directions, respectively; $\overline{Q}_1$ and $\overline{Q}_2$ are the water depth-integrated baroclinic terms in the x and y directions, respectively; τ_{s1}, τ_{s2} and τ_{b1}, τ_{b2} are the surface and bottom components of shear stress in the x and y directions; $\overline{v}_H = \int_{-h}^{\zeta} v_H\,\mathrm{d}z$, is the water depth value of v_H.

Figure 1 shows the computational domain and three gauging stations for modelling validations. To satisfy the CFL (Courant–Friedrichs–Lewy) stability criteria, time step for the two-dimensional external mode is set to be 18 s, and the three-dimensional internal mode is 648 s. We used 1:120 000 topographic map from the Ministry of Transport of China to create a digital elevation model, which was used as a reference data set for the model topography (Figure 1). It should be pointed out that Figure 1 shows the exact computational domain. The grid resolutions in the north–south and east–west directions are approximately 1045.5 and 1038.5 m, respectively.

Details of the governing equations can be found in Luyten *et al*. [22]. Here, we used the total variation diminishing scheme, which is able to widely dampen the numerical diffusion and improve the representations of the dynamics and density of the fronts bounding the flow as done by Arnoux-Chiavassa *et al*. [23]. The k–ε turbulence closure model is used to calculate the vertical eddy viscosity. As the semi-diurnal tide, M_2, is the predominant tidal constituent in this area, it is the only M_2 tidal constituent included at the open sea boundary. Thus the surface elevation at the open sea boundary can be expressed as $\zeta = A\cos(\omega t + \varphi_0 - \varphi)$, in which ζ is the surface elevation; A the M_2 tidal amplitude; ω the M_2 tidal frequency; φ_0 the initial phase; φ the M_2 tidal phase [22].

In our present study, the ambient currents (tides) are given at the open boundaries. Tidal open boundary conditions have been very important to a regional tidal model [24–26]. They can usually be obtained from available observations near the open boundaries (tidal gauge data). Control

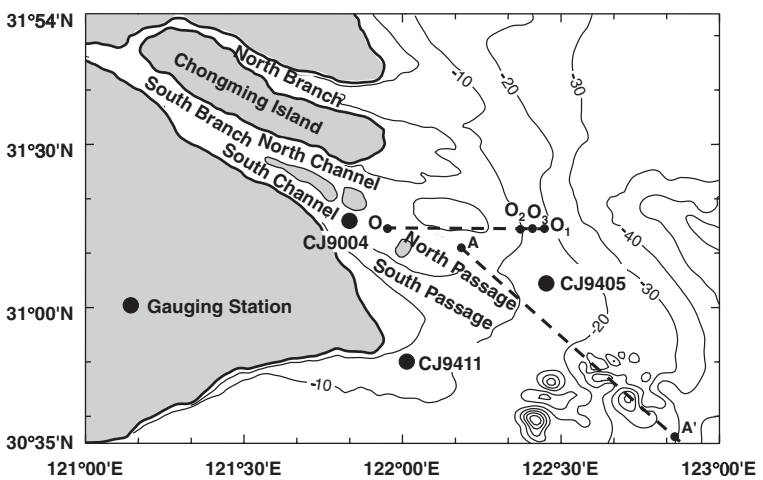

Figure 1. Computational domain, three gauging stations CJ9004, CJ9411, and CJ9405 for modelling validations, and the locations of Line OO_1 and Line AA' within the Changjiang River estuary. The contour lines are in m. Note that Points O_1 (-10 m) and O_2 (-18 m) with an averaged location Point O_3 having a distance about 43 km to Point O.

DOI: 10.1002/fld

variables are the harmonic constants (amplitude and phase) of tidal constituent (M_2) along the open boundary. Linear interpolation has been used to determine the tidal amplitude and phase along the open boundaries. In our present modelling study, the tidal amplitude and phase along the open boundaries have to be determined before computation. These harmonic constants, e.g. the tidal amplitude and phase, were obtained from linear interpolations of co-amplitude and co-tidal lines of M_2 constituent [27].

3. RESULTS AND DISCUSSION

Field experiments were performed by the Shanghai Institute of Waterway Engineering Surveying and Design at stations CJ9004 (121°56′E, 31°15′30″N, 25–26 April 1990), CJ9411 (122°1′22″E, 30°51′03″N, 23–24 November 1994) and CJ9405 (122°27′04″E, 31°05′15″N, 28–29 May 1994) (Figure 1). A spring tide was monitored for 25 h (20:00 h 25 April 1990–21:00 h April 1990), for 13 h (21:00 h 23 November 1994–09:00 h 24 November 1994), and for 28 h (07:00 h 28 May 1994 to 11:00 h 29 May 1994) at three gauging stations CJ9004, CJ9411, and CJ9405, respectively. Current speed and direction were measured hourly at ca. $0.0H$, $0.2H$, $0.4H$, $0.6H$, $0.8H$, and $1.0H$ (H is the total water depth) using an electromagnetic current meter. The surface elevation was interpreted from the water depth measured hourly at the same site.

3.1. Modelling of the current field within the Changjiang River estuary

The first 3 days of the model runs were performed without salinity to initialize the current field. Then, using the observed data from three gauging stations CJ9004 (121°52′38″E, 31°13′30″N, 25–26 April 1990), CJ9411 (122°01′22″E, 30°51′03″N, 23–24 November 1994), and CJ9405 (122°27′04″E, 31°05′15″N, 28–29 May 1994), the model calibration was made to ensure the accuracy of the computation of the current field (Figure 2). The starting times of the runs begin from 3 days before 25 April 1990, 23 November 1994, and 27 May 1994, respectively. Therefore, the exact starting times of the runs began at 20:00 h 22 April 1990, 21:00 h 20 November 1994, and 07:00 h 25 May 1994 (Figure 2). The freshwater discharge was obtained from the Data-sharing Network of China Hydrology (http://www.hydrodata.gov.cn). From the time series in Figure 2, there do not seem to be any initial oscillations that one might expect at the very start of a run if it is started from a state of rest. The run is actually started from a state of rest. That is to say, an initial current/elevation field was not imposed but the obtained current/elevation field after 3 day run was set up as an initial current/elevation field.

Figure 2 shows a comparison between modelled and measured results for (a) surface elevation, (b) depth-averaged current speed, and (c) current direction during 25–26 April 1990, 23–24 November 1994, and 28–29 May 1994 at three gauging stations CJ9004, CJ9411, and CJ9405 (in the dispersal direction of the plume), respectively.

The current characteristics at the gauging stations CJ9004 and CJ9411 are similar (Figure 2). Modelled results show tidal asymmetries at the two stations: (1) the flood phase is about an hour shorter than the ebb phase (the left and middle column (a) in Figure 2); (2) ebb tidal velocity is larger than flood tidal velocity. There is about an hour lag between high slack water and maximum flood tidal velocity, and 2-h lag between low slack water and maximum ebb tidal velocity (the left and middle column (b) in Figure 2); (3) modelled current directions suggest that the currents at the two stations move forwards and backwards with tide, and a transitional point occurs 2 h after

DOI: 10.1002/fld

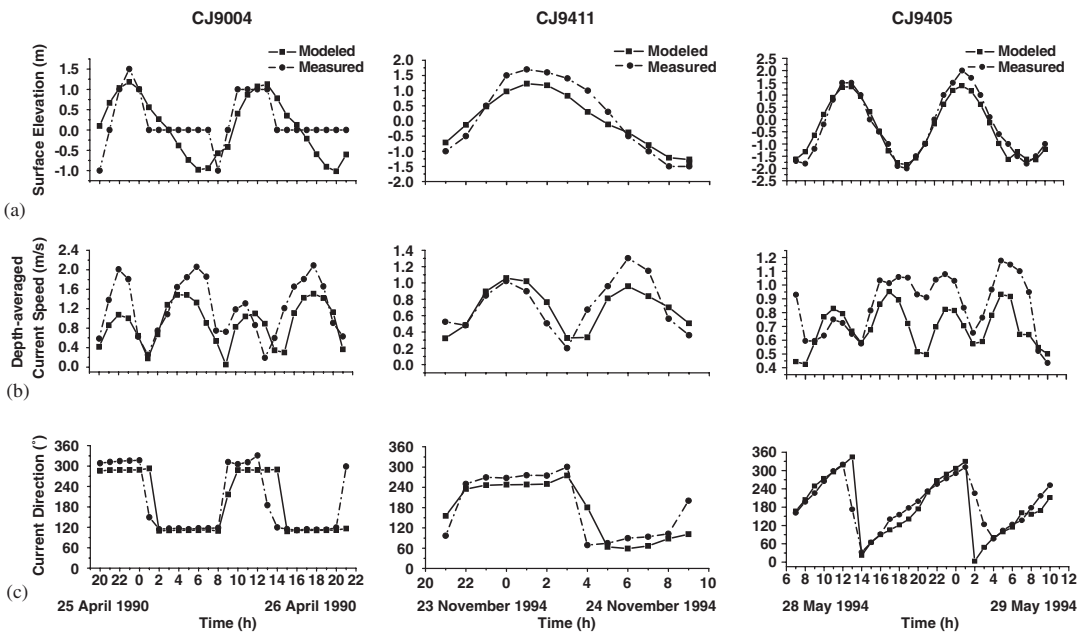

Figure 2. Comparisons between modelled and measured results for: (a) surface elevation; (b) depth-averaged current speed; and (c) current direction during 25–26 April 1990, 23–24 November 1994, and 28–29 May 1994 at three gauging stations CJ9004, CJ9411, and CJ9405, respectively.

the slack water (the left and middle column (c) in Figure 2). As shown in Figure 2, there is a discrepancy between modelled and observed data at the station CJ9004. The observed data at the station CJ9004 have horizontal flat sections while the modelled ones do not. It is unclear what caused them.

Modelled results at the station CJ9405 show that (1) the flood phase is comparable with the ebb phase (the right column (a) in Figure 2); (2) ebb tidal velocity is larger than flood tidal velocity. There is about a 2-h lag between high slack water and maximum flood tidal velocity, and between low slack water and maximum ebb tidal velocity (the right column (b) in Figure 2); (3) current directions suggest that the currents at the station CJ9411 are clockwise. The current direction of the maximum flood velocity is about 280°, and that of the maximum ebb velocity is about 100° (the right column (c) in Figure 2).

Obviously, the observed elevation and currents must include fluctuations that are NOT related to tides and freshwater discharge (e.g. wind-induced component and so forth). Hence, the observed time series in Figure 2 are unlikely to coincide with the modelled ones.

3.2. Horizontal structure of the Changjiang River plume in the summer

The freshwater discharge of the Changjiang exhibits a remarkable seasonal variation. In our present modelling study, as stated above, we do not impose the annually averaged discharge, but one season only, in the summer (flood season). This is due to the fact that the Changjiang River plume appears to be predominant in the summer [13, 16].

DOI: 10.1002/fld

The computation begins from zero and runs for 3 days in order to initialize the flow field. From the 4th day of the simulation, fresh water with the discharge of 49 500 m^3/s (for summertime averaged over multiple years) is released from the west boundary to simulate the dispersal processes of the Changjiang River plume. According to Beardsley *et al*. [13], most Changjiang River discharge is released through the North Channel and the South Channel. The 32 psu isohaline is taken as the eastern boundary of the Changjiang River plume.

It seems likely that the computation ends after 30 days from the beginning. In fact, the observed data from three gauging stations CJ9004, CJ9411, and CJ9405, were firstly used to calibrate the model, in order to ensure the accuracy of the computation of current field (Figure 2). During each calibration, the model was run for 3 days to initialize the current field. Then, 3 days of the model runs were performed without salinity to initialize the current field. Finally, on the basis of those obtained current fields, assuming the reference salinity 32 psu for the whole computational domain but no salinity at the river boundary, the salinity distributions were modelled for 27 days under the combined river runoff and tide (Figure 3). This is simply because of that the Changjiang River plume appears to be fully developed approximately after 27 days modelling.

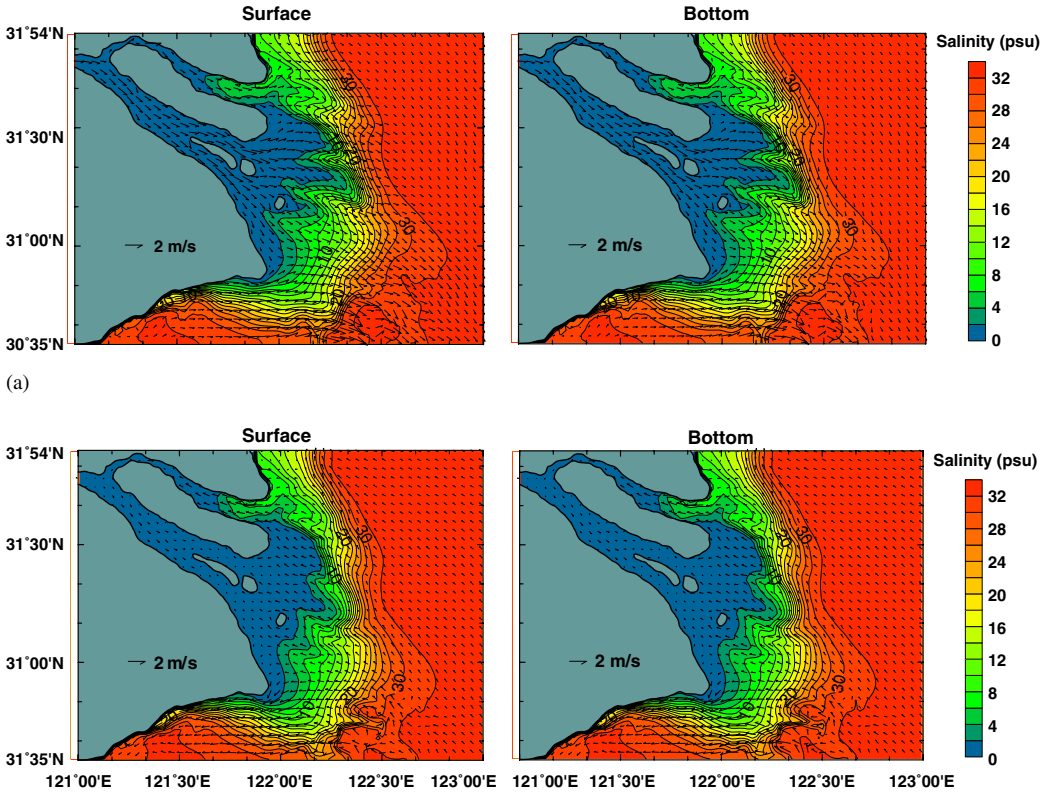

Figure 3. Horizontal distributions of modelled surface and bottom current velocity vectors and salinity fields during (a) maximum ebb tide and (b) maximum flood tide within the Changjiang River plume on the 30th day of the simulation.

DOI: 10.1002/fld

Figure 3 shows the horizontal distributions of modelled surface current vectors and salinity fields during the maximum ebb tide within the Changjiang River plume on the 30th day of the simulation. To present a clear view of the horizontal distribution of modelled velocity vectors, some of them have been neglected in Figure 3. That is to say, only some of the mesh points are indicated by vectors in Figure 3. Therefore, there are differences in mesh points between Figures 1 and 3. Results show: (1) only a small percentage of fresh water is discharged into the North Passage (Figure 3). Consequently, the current velocities are relatively small, while the salinities are high at the North Branch; (2) fresh water is discharged mostly into the South Branch, and mixed with sea water outside the North Channel, the North Passage, and the South Passage, which forms the Changjiang River plume expanding southeastwards; and (3) the horizontal salinity gradients outside the North Channel and the North Passage increase greatly during the maximum ebb tide, and two major plume tongues are formed (Figure 3).

The computation ends before reaching a quasi-steady-state for the present domain (Figure 3). This might be due to the constrained computational domain, i.e. the development or dispersal processes of the Changjiang River plume would be constrained by the open boundaries. Furthermore, the development of the Changjiang River plume seems to be different at the different passages of the Changjiang River estuary, while a quasi-steady-state is reached at the North Channel and North Passage (Figure 3).

The wind-induced current could have played an important role in the shallow estuary, e.g. Tampa Bay [28]. However, the Changjiang River estuary is generally tide-dominated. No attempt will be made to summarize the hydrodynamics of the Changjiang River plumes. For the sake of simplicity, rather the aim of our present study is to focus on the tide-modulated Changjiang River plume.

We would be interested in other processes related to the Changjiang River plume behaviour, e.g. in summer when the monsoon winds are relatively weak. Clearly, our present preliminary studies have neglected the influence of the heat flux through the sea surface. This should be a part of our future studies.

3.3. Vertical structure of the Changjiang River plume along Line AA′

Along the dispersal direction of the Changjiang River plume, Figure 4 shows the vertical distributions of modelled current vectors and salinity fields during (a) maximum ebb tide and (b) maximum flood tide along the line AA′ (Figure 1) on the 30th day of the simulation. Results show that (1) the velocity of plume water during the maximum ebb tide is larger than that of ambient sea water, and during the maximum flood tide the two velocities are similar; (2) the salinity within the Changjiang plume is homogeneous vertically due to strong tidal mixing, from which we can deduce that the type of plume front is surface-to-bottom type according to Narayanan and Garvine's [29] classification.

The model results show uniform salinity from surface to sea bed as shown in Figure 4. This is somewhat different from that the plume in the summer is confined to a thin surface layer 10–15 cm thick in the literature, e.g. Lie *et al*. [19]. This is the influence of the wind. Our present model investigation is looking at the tide-modulated Changjiang River plume, but the surface plume might be due to wind only. Furthermore, parameterizations in the turbulence model might have influenced the vertical structure of salinity. Winds should be taken into account in the future studies.

3.4. Analysis of movement of the Changjiang River plume front

From the outlet of the South Channel (Figure 1), we draw a longitudinal line OO_1 in order to analyse the movement of the plume front. The maximum surface horizontal salinity gradient (used

DOI: 10.1002/fld

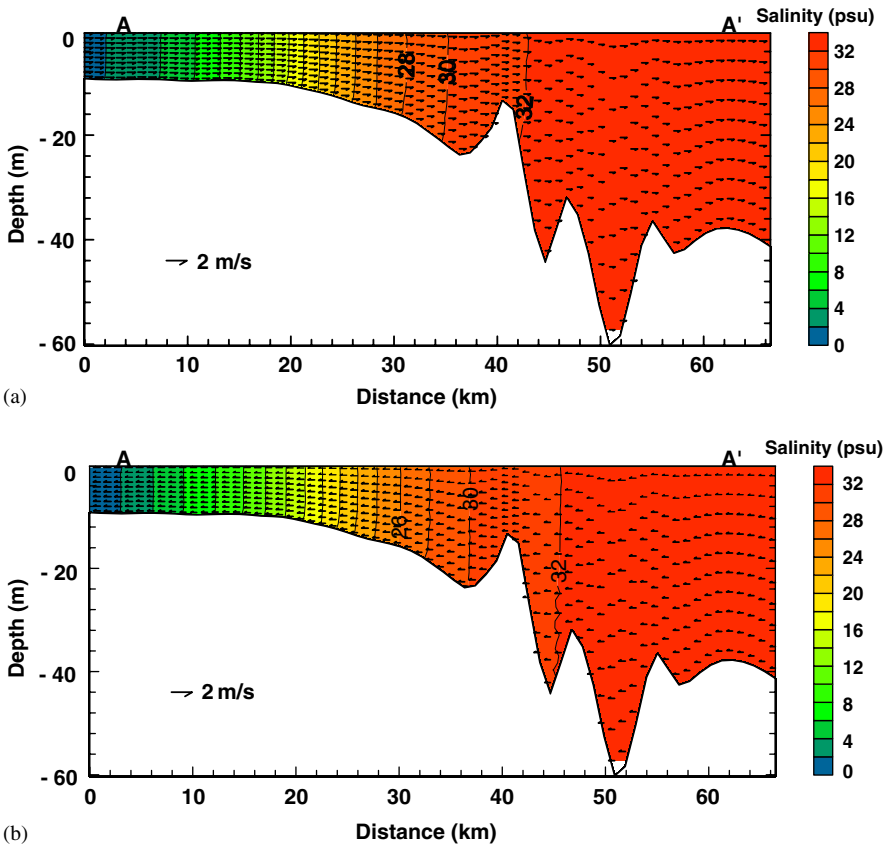

Figure 4. Vertical distributions of modelled current velocity vectors and salinity fields during (a) maximum ebb tide and (b) maximum flood tide along Line AA′ on the 30th day of the simulation.

as the plume front intensity) is calculated as the location of the front. The distance between Point O and the easternmost point of the 32 psu isohaline is defined as the plume length.

Figure 5 shows the hourly time series of the plume length and its linear fit line, and the location of the front. Results show: (1) after the model is run for about three and a half days, the plume reaches to the outlet of the South Channel. Then the plume length begins to increase approximately linearly (curve a in Figure 5); (2) the linear fit for curve a has a slope of 3.38 km/day, which represents the averaged propagating rate of the Changjiang River plume (line b in Figure 5); and (3) the location of the front varies periodically through time. On the 11th day of the simulation, it increases abruptly, then tends to be stable after the 14th day of the simulation, swinging between Points O_1 (−10 m) and O_2 (−18 m) (Figure 1) with an averaged location O_3 having a distance about 43 km to Point O. Similar features have been reported in other tidal estuaries, e.g. the Pearl River estuary [8], China; the Amazon River estuary [2], Brazil. By using numerical modelling, Chapman and Lentz [30] explained that when a steady balance is established in the bottom boundary layer between vertical mixing and onshore advection of density, the front will be trapped to an isobath.

DOI: 10.1002/fld

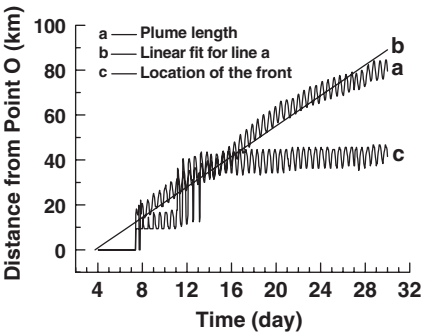

Figure 5. Hourly time series of the Changjiang River plume length (curve a) and its linear fit line (line b), and location of the front (curve c). Note that time (day) refers to day of the simulation.

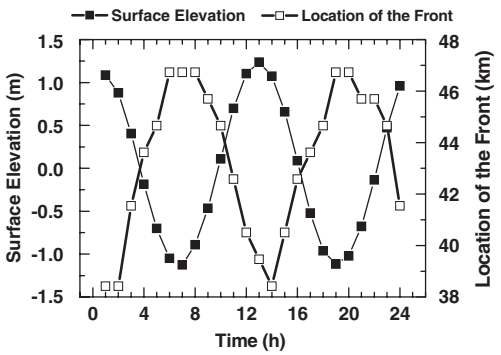

Figure 6. Hourly time series of modelled surface elevation at Point O_3 and the location of the plume front on the 30th day of the simulation.

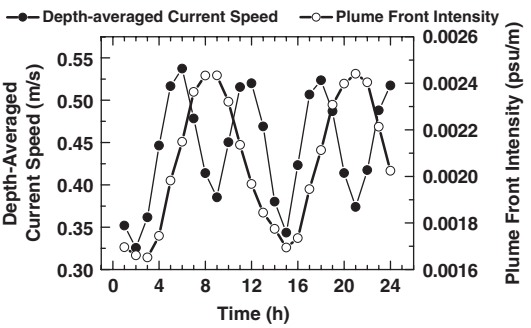

Figure 7. Hourly time series of the depth-averaged current speed at Point O_3 and the plume front intensity on the 30th day of the simulation.

DOI: 10.1002/fld

Figure 6 shows the hourly time series of the surface elevation at the front averaged location O_3 and the location of the front on the 30th day of the simulation. Results show: (1) the plume length varies periodically through time with the same period of the tide; (2) the maximum plume length occurs about 2 h after low slack water and the minimum plume length during high slack water.

Figure 7 shows the hourly time series of the depth-averaged current speed at Point O_3 and the plume front intensity on the 30th day of the simulation. Results show: (1) the plume front intensity varies periodically through time, with the same period of the tide; (2) the maximum plume front intensity occurs during high slack water and the minimum plume front intensity during low slack water.

4. CONCLUSIONS

In this study, after the validation of the current field, the dispersal processes of the tide-modulated Changjiang River plume were numerically modelled. The following conclusions can be drawn from our modelled results:

(1) The plume length increases approximately linearly through time. This implies that the Changjiang River plume is unsteady and grows continually. The linear fit line reveals that its averaged propagating rate is about 3.38 km/day.
(2) The location of the front varies periodically through time, swinging between Points O_1 (-10 m) and O_2 (-18 m).
(3) The horizontal distributions of modelled surface current vectors and salinity fields show that three plume tongues are formed outside the North Channel, the North Passage, and the South Passage, especially during the maximum ebb tide. As a whole, the Changjiang River plume expands southeastwards. The larger horizontal salinity gradient outside the North Channel and the North Passage form a strong plume front.
(4) The vertical distributions of modelled current vectors and salinity fields along the line AA' show that the velocity within the plume during the maximum ebb tide is larger than that within the ambient sea water, and the two velocities are similar during the maximum flood tide. The salinity within the Changjiang River plume is homogeneous vertically due to strong tidal mixing, from which we can deduce that the plume front is of a surface-to-bottom type.
(5) Being modulated by the tide, both plume location and plume front intensity vary periodically. The maximum plume length occurs about 2 h after low slack water and the minimum plume length during high slack water. The maximum plume front intensity occurs during high slack water and the minimum plume front intensity during low slack water.

In future studies, more factors should be taken into account, such as the monsoon winds, which contributes to the de-stratification or mixing within the Changjiang River plume.

ACKNOWLEDGEMENTS

This study was jointly supported by the National Science Fund for Distinguished Young Scholars (Estuarine and Coastal Science 40225014) and the National Natural Science Foundation of China (Hydraulic Science 50679040). Hua-Jun Zhou, Shu-Ying Zhang and the Shanghai Institute of Waterway Engineering Surveying and Design are thanked for providing us with the hydrographic data. Fang-Xi Hu of East China Normal

DOI: 10.1002/fld

University is thanked for his advice on our research. P. Luyten, from the Management Unit of the North Sea Mathematical Models, is thanked for providing us with the COHERENS. Two anonymous reviewers are thanked for their constructive comments.

REFERENCES

1. Dyer KR. *Estuaries. A Physical Introduction* (2nd edn). Wiley: Chichester, 1997; 195.
2. Lentz SJ, Limeburner R. The Amazon River plume during AMASSEDS: spatial characteristics and salinity variability. *Journal of Geophysical Research* 1995; **100**(C2):2355–2375.
3. Park K. Columbia River plume identification by specific alkalinity. *Limnology and Oceanography* 1966; **11**(1): 118–120.
4. Nash JD, Moum JN. River plumes as a source of large-amplitude internal waves in the coastal ocean. *Nature* 2005; **437**:400–403.
5. Orton PM, Jay DA. Observations at the tidal plume front of a high-volume river outflow. *Geophysical Research Letters* 2005; **32**:L11605 (DOI: 10.1029/2005GL022372).
6. Garvine RW. Physical features of the Connecticut River outflow during high discharge. *Journal of Geophysical Research* 1974; **79**(6):831–846.
7. Garvine RW. Observations of the motion field of the Connecticut River plume. *Journal of Geophysical Research* 1977; **82**(3):441–454.
8. Dong LX, Su JL, Wong LA, Cao ZY, Chen JC. Seasonal variation and dynamics of the Pearl River plume. *Continental Shelf Research* 2004; **24**:1761–1777.
9. Van Alphen JSLJ, De Ruijter WPM, Borst JC. Outflow and three-dimensional spreading of Rhine River water in the Netherlands coastal zone. In *Physical Processes in Estuaries*, Dronkers J, van Leussen W (eds). Springer: Berlin, Heidelberg, 1988; 70–92.
10. Ruddick KG, Deleersnijder E, De Mulder T, Luyten PJ. A model study of the Rhine discharge front and downwelling circulation. *Tellus* 1994; **46A**:149–159.
11. de Boer GJ, Pietrzak JD, Winterwerp JC. On the vertical structure of the Rhine region of freshwater influence. *Ocean Dynamics* 2006; **56**:198–216.
12. Broche P, Devenon J-L, Forget P, De Maistre J-C, Naudin J-J, Cauwet G. Experimental study of the Rhone plume. Part I: Physics and dynamics. *Oceanologica Acta* 1998; **21**(6):725–738.
13. Beardsley RC, Limeburner R, Yu H, Cannon CA. Discharge of the Changjiang (Yangtze River) into the East China Sea. *Continental Shelf Research* 1985; **4**(1–2):57–76.
14. Su JL, Wang KS. Changjiang River plume and suspended sediment transport in Hangzhou Bay. *Continental Shelf Research* 1989; **9**(1):93–111.
15. Chang P-H, Isobe A. A numerical study on the Changjiang diluted water in the Yellow and East China Seas. *Journal of Geophysical Research* 2003; **108**(C9):1–17.
16. Beardsley RC, Limeburner R, Hu DX, Le KT, Cannon GA, Pashinski DJ. Structure of the Changjiang River Plume in the East China Sea during June 1980. *Proceedings of International Symposium on Sedimentation on the Continental Shelf with Special Reference to the East China Sea*, Hangzhou, China, vol. 1. China Ocean Press: Beijing, 12–16 April 1983; 243–260.
17. Zhang QH, Janowitz GS, Pietrafesa LJ. The interaction of estuarine and shelf waters: a model and applications. *Journal of Physical Oceanography* 1987; **17**:455–469.
18. Bang I, Lie H-J. A numerical experiment on the dispersal of the Changjiang River plume. *Journal of the Korean Society of Oceanography* 1999; **34**(4):185–199.
19. Lie H-J, Cho C-H, Lee J-H, Lee S. Structure and eastward extension of the Changjiang River plume in the East China Sea. *Journal of Geophysical Research* 2003; **108**(C3):3077 (DOI: 10.1029/2001JC001194).
20. Wang BD. Cultural eutrophication in the Changjiang (Yangtze River) plume: history and perspective. *Estuarine, Coastal and Shelf Science* 2006; **69**:471–477.
21. Lu LF, Shi JZ. On the dispersion of the tide-modulated Changjiang River plume, China: a numerical study. *Proceedings of the 2nd International Conference on Estuaries and Coasts*, Guangzhou, 28–30 November 2006, vol. II. Guangdong Economy Publishing House: China, 2006; 1072–1079.
22. Luyten PJ, Jones JE, Proctor R, Tabor A, Tett P, Wild-Allen K. COHERENS—A COupled Hydrodynamical–Ecological model for REgional and Shelf Seas: User Documentation. *MUMM Report*, Management Unit of the Mathematical Methods of the North Sea, Belgium, 1999; 914.

23. Arnoux-Chiavassa S, Rey V, Fraunié P. Modeling 3D Rhone river plume using a higher order advection scheme. *Oceanologica Acta* 2003; **26**:299–309.
24. Fang GH, Yang JF, Thao YC. A two-dimensional numerical model for tidal motion in the Taiwan Strait. *Marine Geophysical Researches* 1984; **7**:267–276.
25. Shi Z, Li SS, Petersen OS. A vertically moving grid finite element modeling of tidal flow in the Changjiang Estuary, China. *International Journal for Numerical Methods in Fluids* 2003; **43**(2):115–127.
26. Zhang AJ, Wei E, Parker BB. Optimal estimation of tidal open boundary conditions using predicted tides and adjoint data assimilation technique. *Continental Shelf Research* 2003; **23**:1055–1070.
27. ECNU. *Report on Comprehensive Investigation of the Coastal Zone and Tidal Flat in Shanghai*. Shanghai Science and Technology Publishing House: Shanghai, China, 1988.
28. Shi JZ, Luther ME, Meyers S. Modelling of wind wave-induced bottom processes during the slack water periods in Tampa Bay, Florida. *International Journal for Numerical Methods in Fluids* 2006; **52**(11):1277–1292.
29. Narayanan C, Garvine RW. Large scale buoyancy driven circulation on the continental shelf. *Dynamics of Atmospheres and Oceans* 2002; **36**:125–152.
30. Chapman DC, Lentz SJ. Trapping of a coastal density front by the bottom boundary layer. *Journal of Physical Oceanography* 1994; **24**:1464–1479.

DOI: 10.1002/fld